Journal of the European Ceramic Society **10** (1992) 245–253

Sintering of Nanocrystalline ZrO_2 and Zirconia Toughened Alumina (ZTA)

Ha-Young Lee, Werner Riehemann & Barry Leslie Mordike

Institut für Werkstoffkunde und Werkstofftechnik, Technische Universität Clausthal, Agricolastrasse 6, D-3392 Clausthal-Zellerfeld, Germany

(Received 2 December 1991; revised version received 3 January 1992; accepted 28 February 1992)

Abstract

Ultrafine oxide powders of ZrO_2 and MgO were produced by laser ablation. The pure atomised powders and mixtures thereof were heated up to temperatures between 600 and 1600°C. The tetragonal phase in pure ZrO_2 powder transformed continuously between approximately 400 and 1000°C to the monoclinic phase. On addition of 5 vol.% MgO the transformation temperature could be increased by about 400 K and grain growth suppressed. Dilatometer measurements on compressed powder specimens showed that the shrinkage curve for nanocrystalline ZrO_2 was depressed by 300 K relative to a microcrystalline ZrO_2 specimen. The ZrO_2 specimen with 5 vol.% MgO was isostatically pressed and sintered in the temperature range 1000–1500°C. Sintered specimens contained 20–50% of the tetragonal phase. The specimen sintered at 1250°C for 1 h achieved a relative density of 95%. Small increases above this were observed in specimens sintered between 1250 and 1500°C. The 90 vol.% Al_2O_3 + 10 vol.% ZrO_2 (with 5 vol.% MgO) specimens were also sintered in the temperature range 1400–1600°C. The specimens achieved high density (98%), microhardness (17·8 GPa) and toughness (7·2 MPa $\sqrt{m}$).

Es wurden ultrafeine ZrO_2- und MgO-Pulver durch Laserabtrag hergestellt. Die reinen atomisierten Pulver und deren Mischungen wurden auf Temperaturen zwischen 600 und 1500°C aufgeheizt. Zwischen etwa 400 und 1000°C wandelte sich die tetragonale Phase des reinen ZrO_2-Pulvers kontinuierlich in die monokline Phase um. Bei einer MgO-Zugabe von 5 Vol.% konnte die Umwandlungstemperatur um etwa 400 K gesteigert und das Kornwachstum unterdrückt werden. Dilatometermessungen an verpreßten Pulverproben zeigten, daß die Schrumpfungskurve für nanokristallines ZrO_2 gegenüber einer mikrokristallinen Probe um 300 K herabgesenkt ist. ZrO_2-Proben mit 5 Vol.% MgO-Zusatz wurden isostatisch verpreßt und im Temperaturbereich zwischen 1000 und 1500°C gesintert. Die gesinterten Proben enthielten 20 bis 50% der tetragonalen Phase. Eine Probe, die für 1 h bei 1250°C gesintert wurde, erreichte eine relative Dichte von 95%. Für Proben, die zwischen 1250 und 1500°C gesintert wurden, konnten geringe Steigerungen über diesen Wert hinaus beobachtet werden. Proben mit 90 Vol.% Al_2O_3 und 10 Vol.% ZrO_2-Anteil (und 5 Vol.% MgO-Zusatz) wurden im Temperaturbereich zwischen 1400 und 1600°C gesintert. Diese Proben erreichten eine hohe Dichte (98%), eine hohe Mikrohärte (17·8 GPa) und eine hohe Zähigkeit (7·2 MPa $\sqrt{m}$).

Des poudres ultrafines de ZrO_2 et MgO ont été produites par ablation laser. Pour cela les poudres et les mélanges atomisés purs ont été chauffés a des températures variant entre 600 et 1600°C. La phase tetragonale de la poudre de ZrO_2 pure s'est transformée de façon continue entre 400 et 1000°C en phase monoclinique. Par l'addition de 5 vol.% de MgO, la température de transformation a pu être élevée de 400 K et la croissance de grain supprimée. Les mesures de dilatomètre sur des échantillons compressés montrent que la courbe de retrait pour du ZrO_2 nanocristallin a été abaissée de 300 K par rapport à l'échantillon de ZrO_2 microcristallin. L'échantillon de ZrO_2 avec 5 vol.% de MgO a été compacté isostatiquement et fritté dans un domaine de température compris entre 1000 et 1500°C. Les échantillons frittés contiennent 20 à 50% de phase tetragonale. L'échantillon fritté à 1250°C pendant 1 h présente une densité relative de 95%. D'un peu meilleurs résultats ont été observés pour les échantillons frittés entre 1250 et 1500°C. Les échantillons 90 vol.% Al_2O_3 +

Journal of the European Ceramic Society 0955-2219/92/$5.00

10 vol.% ZrO_2 (avec 5 vol.% de MgO) ont aussi été frittés entre 1400 et 1600°C. Ces échantillons présentent une haute densité (98%), une microdureté de 17·8 GPa et une tenacité de 7·2 MPa$\sqrt{m}$.

1 Introduction

Two strengthening mechanisms can be proposed for nanocrystalline ZrO_2, both of which are based on the concept of hindering crack initiation and growth. The first model relies on the small particle size. It is generally known that strength increases with decreasing particle size. If the grain size is of the order of 10 nm the volume of the grains is about the same as that of the grain boundaries.[1,2] Completely different properties are thus expected for nanocrystalline materials compared to coarse grain materials.[3,4] The increased grain boundary diffusion, for example, enables deformation to take place at low temperatures without crack formation or growth. The second model is based on a phase change from tetragonal to monoclinic ZrO_2.[5] This phase transformation has features similar to the martensite transformation. There are three allotropes of ZrO_2, monoclinic (m), tetragonal (t) and cubic (c). The monoclinic phase is the stable phase at room temperature. If the tetragonal phase can be introduced as inclusions of small size, it can be retained to room temperature; it can then transform under stress associated with the growth of cracks to the monoclinic phase. This phase transformation can arrest crack growth and thus strengthen the material.[6-8] A major feature of research in ZrO_2 systems has thus been the retention or stabilisation of the tetragonal phase.[9]

2 Experimental Details

The laser used for the production of the powder was a NdYAG laser JK701 (Lumonics). The experimental set-up is shown in Fig. 1.

The beam was focused on to the target material which then became atomised. The target was

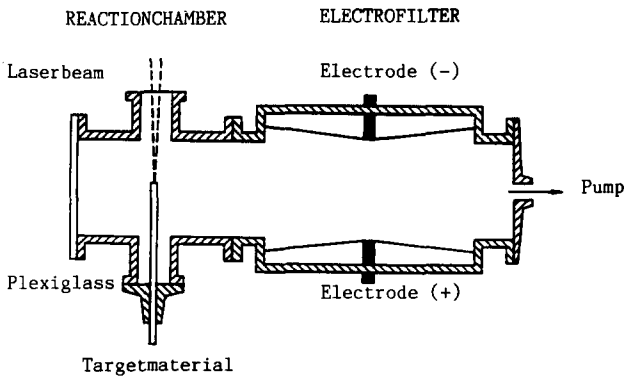

Fig. 1. Experimental set-up.

zirconium wire of 1 mm diameter. The nanocrystalline magnesium was produced from a 10 mm diameter rod. Evaporated metal atoms or clusters react with oxygen in the chamber, resulting in the formation of ultrafine powders. The powder particles were drawn into the electrofilter by a pump. The yield was determined by weighing the electrodes. The structure of the powder was examined using a Siemens X-ray diffractometer D500/501. A quantitative evaluation of the ZrO_2 powder is possible by comparing the peak intensities. The particle size was determined by transmission electron microscopy and in addition by evaluation of X-ray diffraction patterns. In the latter case this involved measuring peak broadening and Fourier analysis using the Crysis programs of Siemens.

Samples of pure ZrO_2 and $ZrO_2 + MgO$ were studied. In order to obtain powder mixtures the pure laser-atomised powders were first mixed under ethanol in an ultrasonic bath for 8–10 min and then dried. Consolidation of powders was carried out by isostatically compressing at 200 MPa and subsequently sintering at a constant heating rate of 5 K/min to a maximum temperature, holding at this temperature for 1, 3 or 5 h and then cooling, also at 5 K/min (specimens ZM). Further specimens were prepared by mixing laser-atomised ZrO_2 powder with 90 vol.% Al_2O_3 (Alcoa, Ludwigshafen, FRG, mean size 0·6 μm) powder, and sintering for 1 h at 1400, 1500 and 1600°C (specimens C). The complete sinter programme is given in Tables 1(a) and 1(b).

Table 1(a). Sinter programme for specimens ZM with the composition 95 vol.% ZrO_2 and 5 vol.% MgO

Time (h)	*Sinter temperature (°C)*							
	1000	*1100*	*1200*	*1250*	*1300*	*1400*	*1500*	*1600*
1	ZM11	ZM12	ZM13	ZM17	ZM14	ZM15	ZM16	ZM18
3	—	—	—	ZM27	ZM24	ZM25	ZM26	ZM28
5	—	—	—	ZM37	ZM34	ZM35	ZM36	ZM38

Table 1(b). Sinter programme for specimens C with the composition 10 vol.% ZM and 90 vol.% Al_2O_3

Time (*h*)	*Maximum sinter temperature* (°C)		
	1400	*1500*	*1600*
1	C1	C2	C3

The density was measured using the water displacement method after infiltrating the specimens with paraffin. The microstructure was examined using a Hitachi X650 scanning electron microscope and the phases analysed by X-ray diffraction. Hardness and fracture toughness were measured using indentation methods.

3 Results and Discussion

3.1 Properties of the ultrafine powder

The as-prepared nanocrystalline ZrO_2 and MgO powders were examined by X-ray diffraction. The

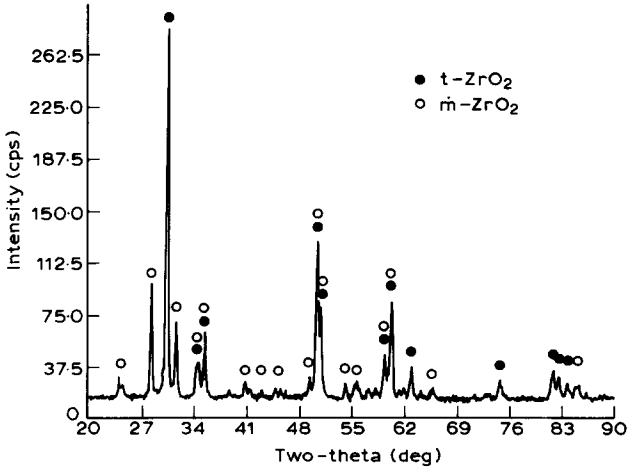

(a)

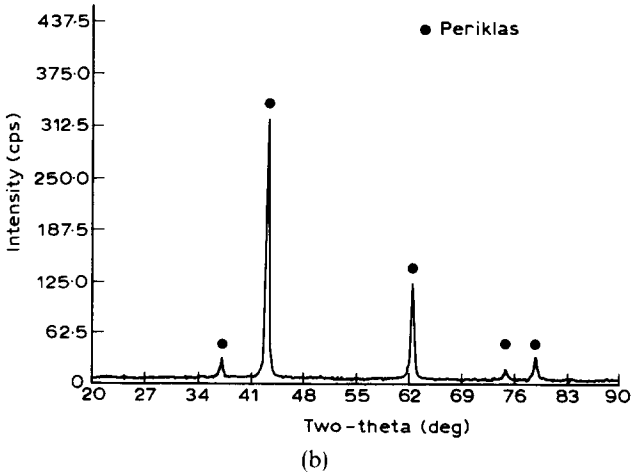

(b)

Fig. 2. (a) X-ray diffraction pattern for ZrO_2; (b) X-ray diffraction pattern for MgO.

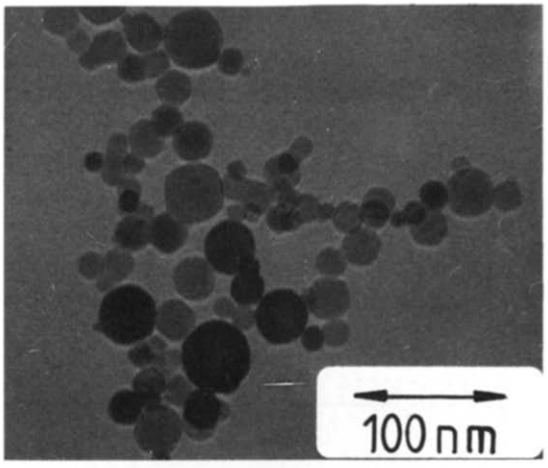

(a)

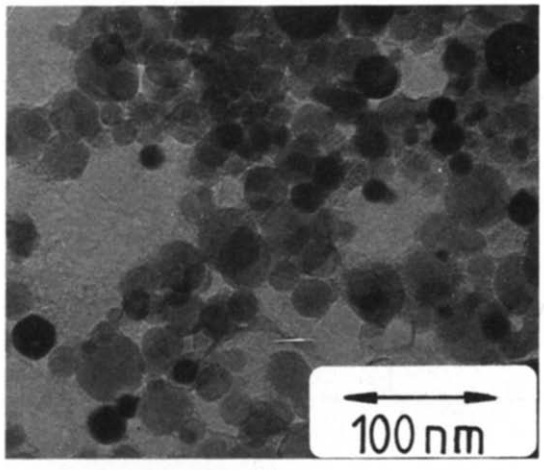

(b)

Fig. 3. (a) TEM micrograph of ZrO_2 powder, bright field, 300 kV; (b) TEM micrograph of MgO powder, bright field, 300 kV.

ZrO_2 powder consisted of tetragonal and monoclinic phases, whereas only one phase, periclase, is observed in MgO, as shown in Fig. 2(a) and (b).

The formation of the tetragonal form of ZrO_2 (stable in bulk above 1100°C) at lower temperatures is due to the fine grain size.[5] The peak intensities of monoclinic (m) ($11\bar{1}$) and (111) and tetragonal (t) (101) peaks were used for determining the amount of the phases present. The intensities were corrected for polarisation.[10,11] It was calculated that 70 vol.% of the tetragonal ZrO_2 phase was present.

The as-produced powders are white. Figure 3(a) and (b) show transmission electron micrographs. Figure 4(a) and (b) give the particle size distributions obtained by evaluating the transmission electron micrographs.

The powders are polyhedron shaped and slightly agglomerated. If a spherical shape is assumed then a log normal distribution of diameters is observed. This result is typical and well known for sublimated particles.[12] The mean particle diameter for ZrO_2

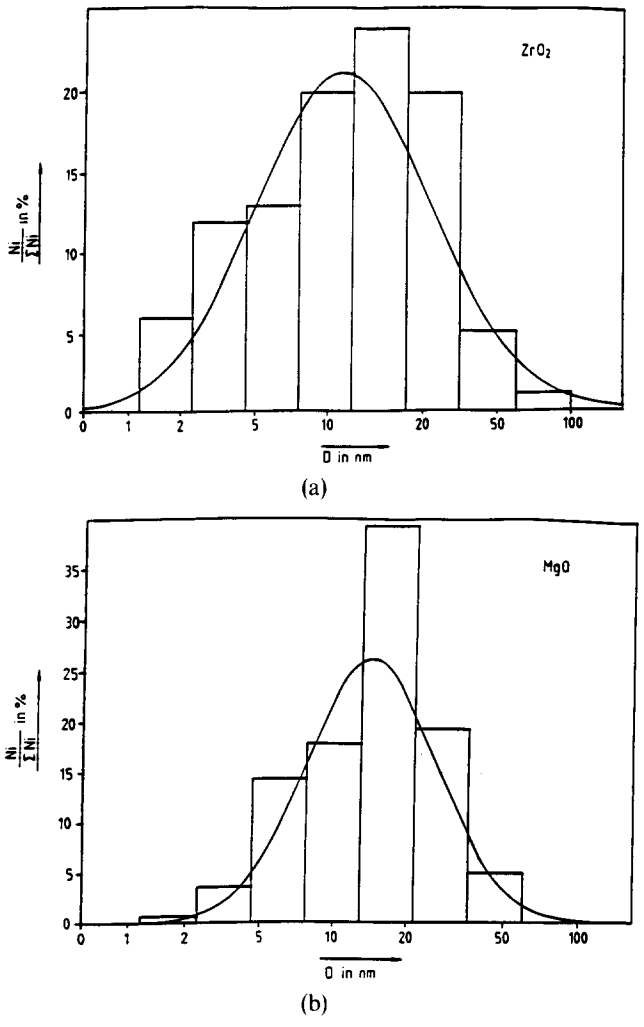

Fig. 4. (a) Size distribution of ZrO_2; (b) size distribution of MgO.

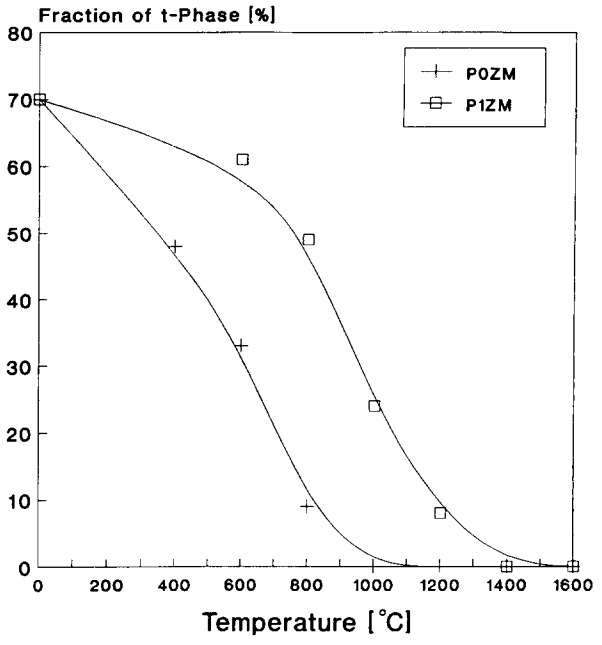

Fig. 5. Phase transformation of ZrO_2 powder on continuous heating as a function of maximum temperature.

powder is 16 nm and for MgO powder 17 nm. It can be seen in Fig. 4(a) and (b) that 95% of particles for both ZrO_2 and MgO lie in the range 1–40 nm. The average values obtained by X-ray diffraction were 17 nm for ZrO_2 and 15 nm for MgO.[13] The two methods are in good agreement. The properties of powder prepared by laser atomisation are given in Table 2.

3.2 Heat treatment of the powders

Loose powder particles were heated at 5 K/min from room temperature to 1600°C and immediately cooled at the same rate. Phase transformations (Fig. 5) and particle growth (Fig. 6) were studied. Figure 6 shows that particle growth in MgO-stabilised specimens is observed at much higher temperature than in pure ZrO_2 specimens. The tetragonal phase of pure ZrO_2 and ZrO_2 + 5 vol.% MgO transforms continuously to the monoclinic phase with increasing temperature. Figure 5 shows that the transformation is also displaced to higher temperatures by the addition of 5 vol.% MgO.

3.3 Sintering of cold pressed powders

Prior to sintering the specimens, dilatometer measurements were made on pressed compacts prepared from coarse grain and nanocrystalline ZrO_2.

Figure 7 shows that the shrinkage curve in a nanocrystalline ZrO_2 is displaced by 300 K to lower temperature compared to coarse-grained ZrO_2 specimens. A decrease in sintering temperature for the nanocrystalline material is to be expected. Specimens which had been isostatically pressed at room temperature were sintered for various periods between 1000 and 1600°C. The densities achieved

Table 2. Properties of laser atomised ZrO_2 and MgO powders

Oxide powder	*Target material*	*Yield (g/h)*	*Volume fractions (%)*	*Powder particles (nm)*	
				TEM	*Diffraction*
ZrO_2	Zr wire ø = 1 mm	3	70 tetragonal 30 monoclinic	16	17
MgO	Mg rod ø = 10 mm	1·1	100 periclase	17	15

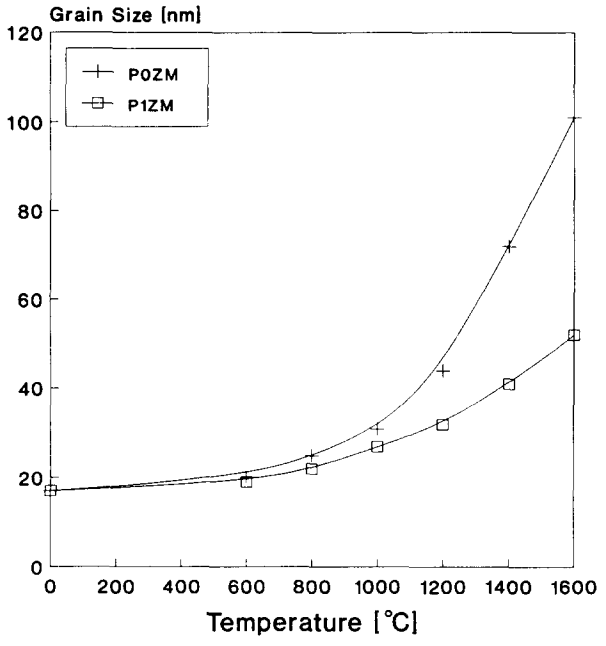

Fig. 6. Particle growth of ZrO_2 powder on continuous heating as a function of maximum temperature.

are shown in Fig. 8(a) and (b) as a function of the sintering temperature.

The maximum density shown in Fig. 8(a) was over 95% of the theoretical density. Figure 9 shows the density of the specimen ZM as a function of sintering time. Figures 8 and 9 show that neither higher sintering temperature nor longer sintering times lead to further densification. Figure 10(a) and (b) show SEM micrographs of fractured sintered specimens.

These figures show higher densities with increasing temperature up to 1250°C. Above 1250°C

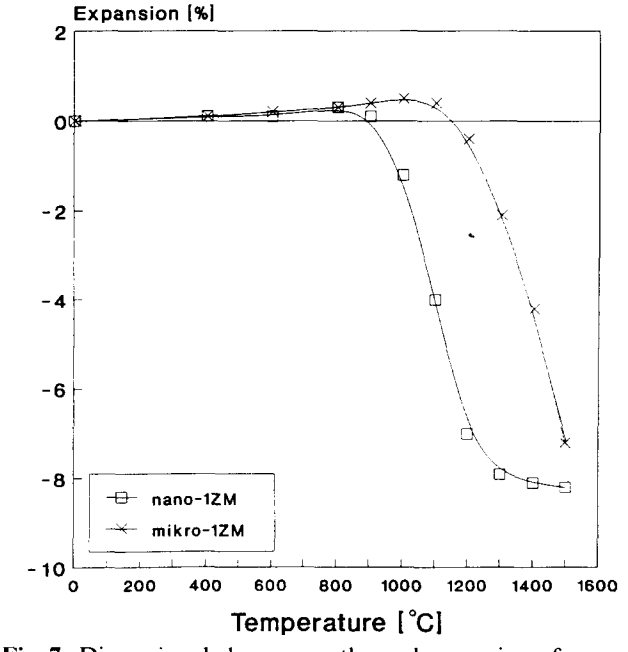

Fig. 7. Dimensional changes on thermal expansion of pressed nano- and micro-crystalline powder. Heating rate: 5 K/min.

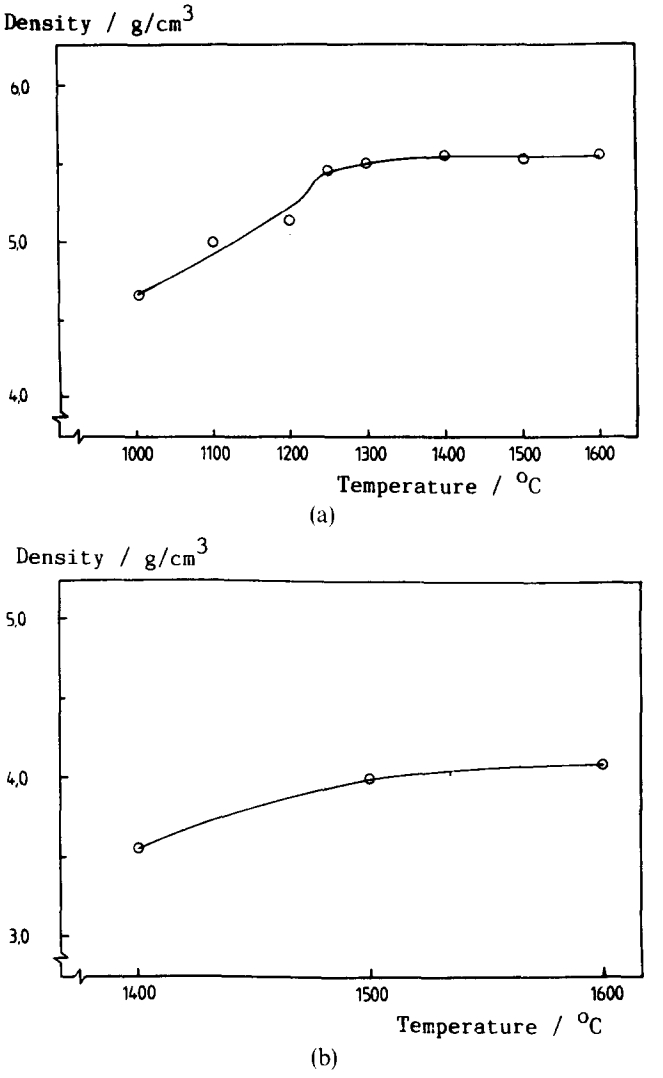

Fig. 8. (a) Density attained in compressed and sintered specimens of type ZM as a function of the sintering temperature; (b) density attained in compressed and sintered type C specimens as a function of the sintering temperature.

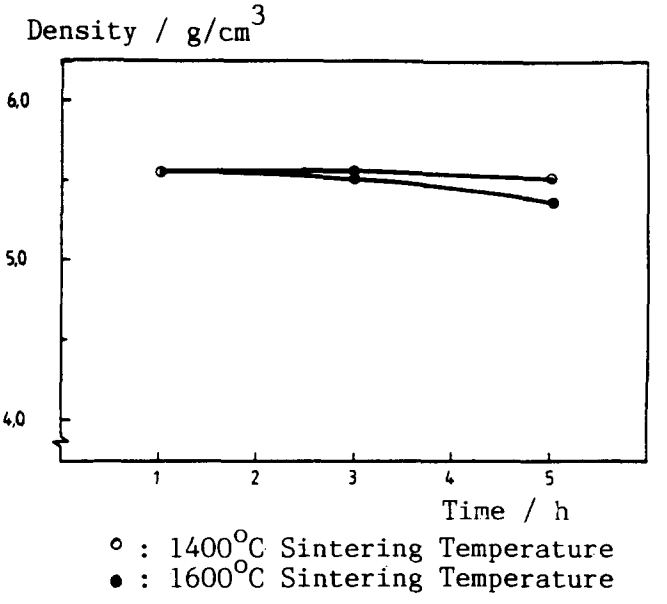

Fig. 9. Density of ZM type specimens heated at 5 K/min to 1400 or 1600°C and holding there for 1, 3 and 5 h.

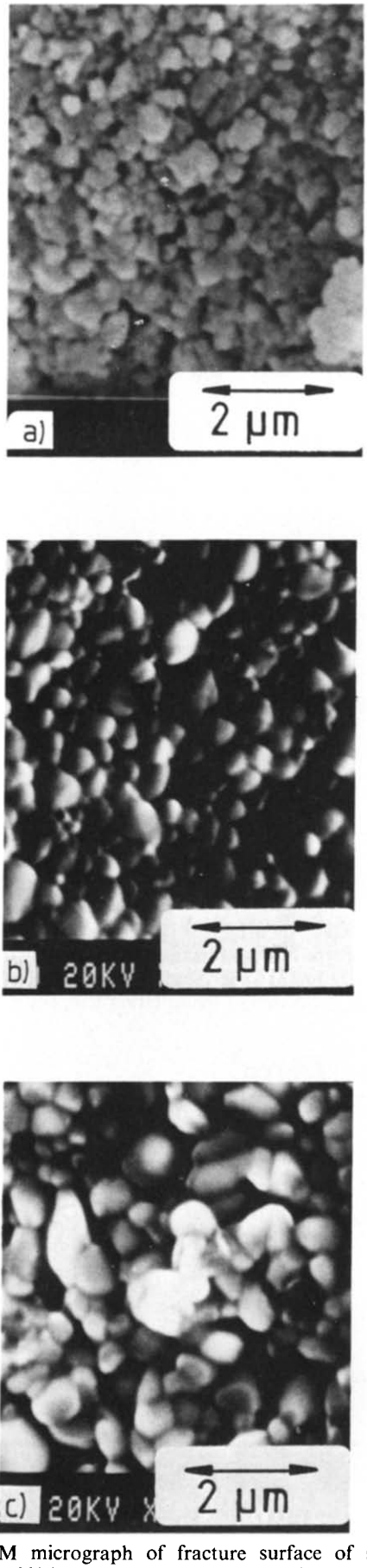

Fig. 10. SEM micrograph of fracture surface of specimen (a) ZM 12 (1100°C, 1 h), (b) ZM 17 (1250°C, 1 h) and (c) ZM 15 (1400°C, 1 h).

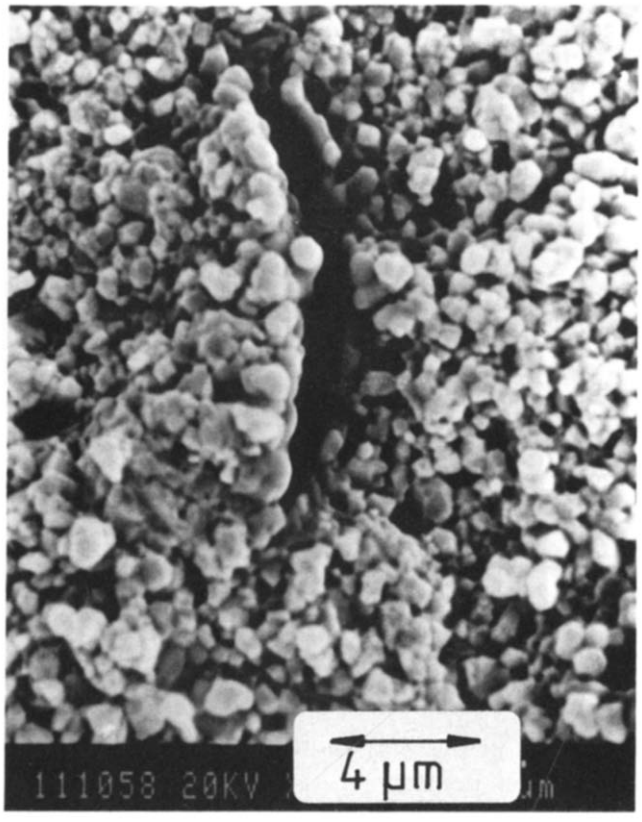

Fig. 11. Scanning electron micrograph showing fracture particle ZM15 (1400°C, 1 h).

further grain growth is observed (Fig. 10(b) and (c)) but no increase in density. The reason could be the low density of the green compact (49% theoretical density) and the fracture of agglomerated and hollow particles (Fig. 11). Hollow particles are produced in laser production of ultrafine particles and these are presumably fractured on compaction.[14–16] The coarse agglomerated particles are present only to a small degree, but due to their large effective volume they prevent the density on sintering from achieving more than 95% of the theoretical density.

The density in the C specimens increased with increasing sintering temperature. The specimen C3 which was sintered for 1 h at 1600°C achieved 98% of the theoretical density. Specimen C3 shows likewise a uniform grain growth (Fig. 12(a) and (b)).

30–50% of the tetragonal phase remains in the ZM specimens after sintering (Fig. 13). This can reach 90% in the C specimens on increasing the sintering temperature.

3.4 Hardness and toughness

The Vickers hardness was measured for a load of 4·9 N (Fig. 14).

The hardness of the ZM specimens (sintered for 1 h) increases strongly with increasing sintering

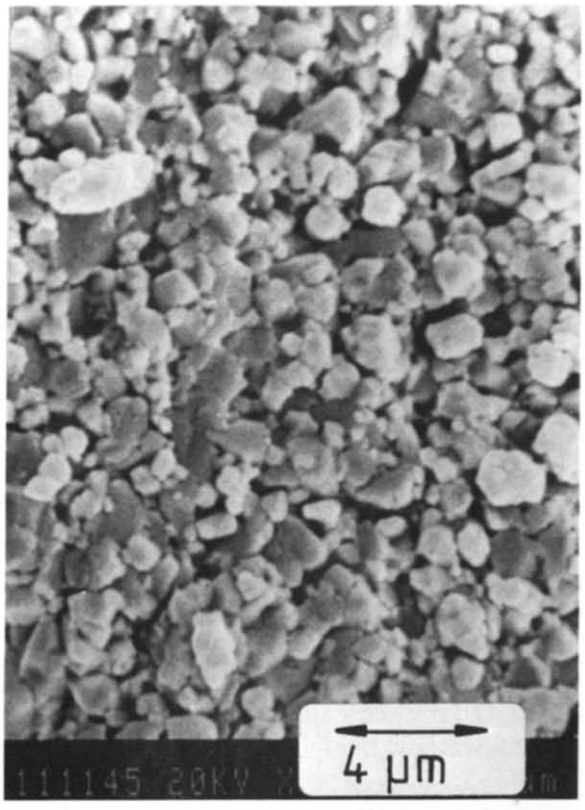

(a)

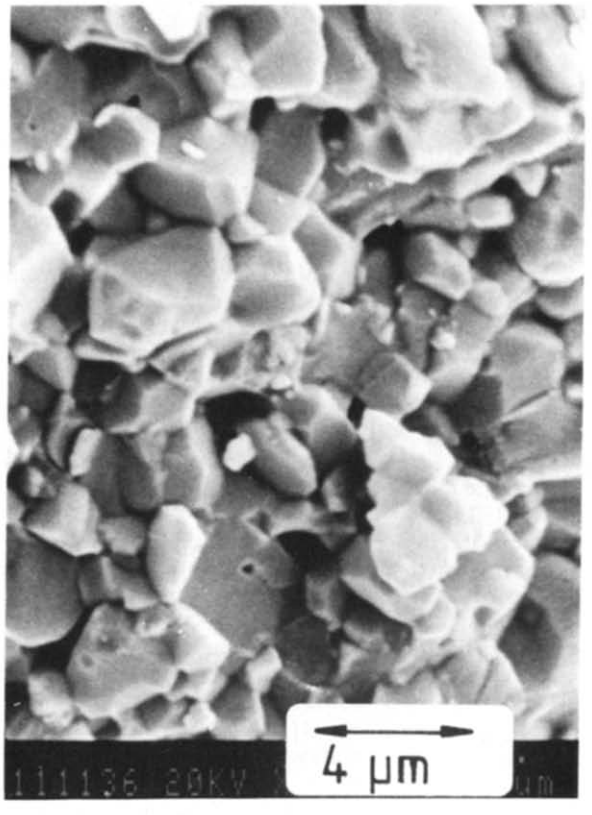

(b)

Fig. 12. (a) Scanning electron micrograph of specimen C2 (1500°C, 1 h), (b) scanning electron micrograph of specimen C3 (1600°C, 1 h).

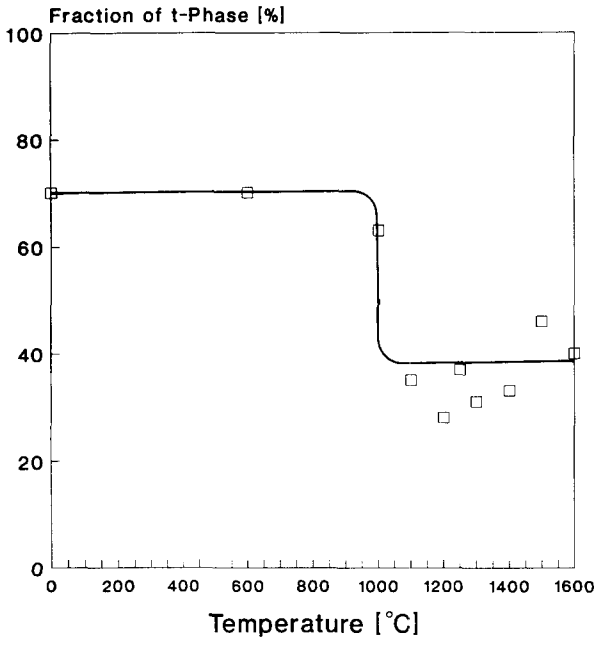

(a)

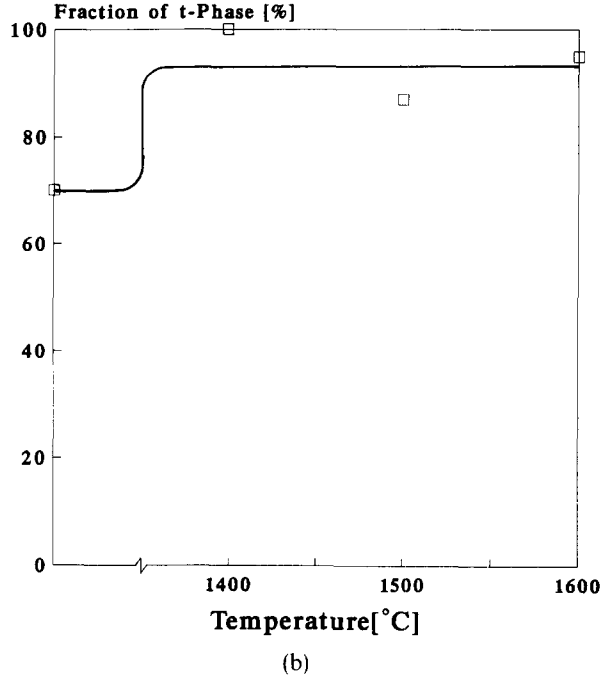

(b)

Fig. 13. (a) Change in volume fraction of the tetragonal phase in ZM specimens on changing the sintering temperature, (b) volume fraction of the tetragonal phase in C specimens at different sintering temperatures.

temperature up to 1300°C, passes through a maximum at 1399–1400°C and thereafter decreases slightly (Fig. 15). The hardness increase is related to the increase in density.

The decrease at high temperatures could be explained by grain growth outweighing the density increase. The maximum hardness of 7·1 GPa was obtained after sintering for 5 h at 1250°C. The hardness of C specimens also increased with

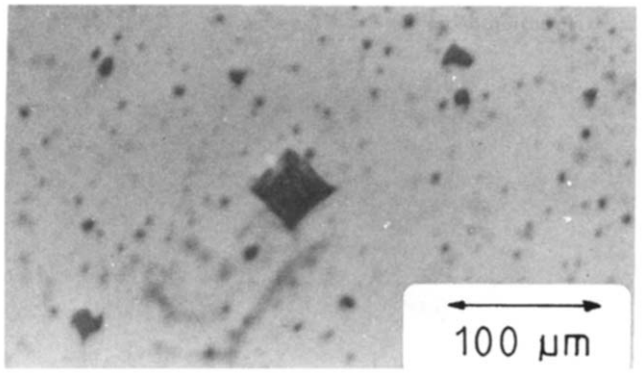

Fig. 14. Hardness test impressions on specimen ZM14 obtained with a load of 4·9 N.

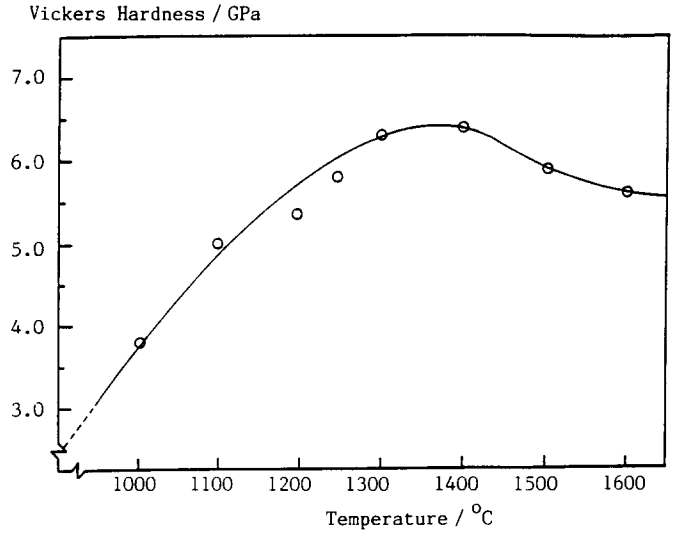

(a)

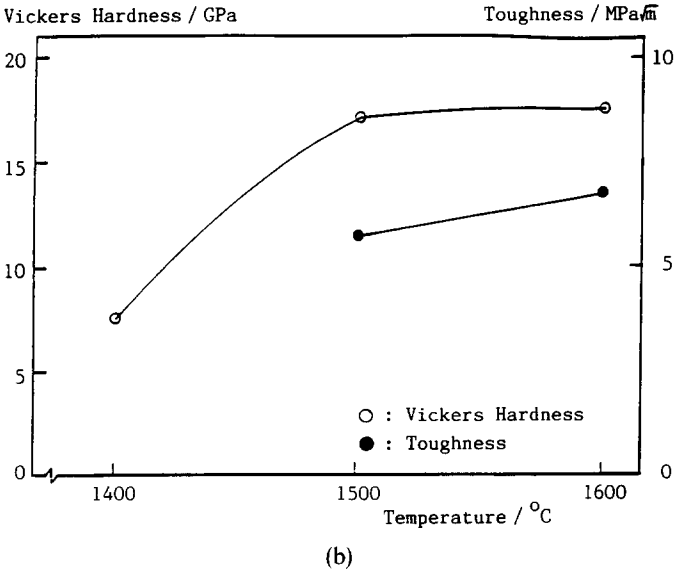

(b)

Fig. 15. (a) Vickers hardness of ZM specimens as a function of sintering temperature for 1 h sintering time, (b) Vickers hardness and fracture toughness as a function of sintering temperature for 1 h sintering time.

increased sintering temperature and attained a maximum hardness of 17·8 GPa. The fracture toughness (K_{IC}) was estimated from the hardness and crack length:

$$K_{IC} = \frac{0{\cdot}47}{\theta} \cdot H_V \cdot \sqrt{C} \cdot \frac{1}{(b/c)^{3/2}}$$

$$\theta = \frac{H_V}{\sigma_B} \cong 3$$

Where $2b$ is the crack and impression length, $2c$ the impression length, H_V the Vickers hardness and σ_B the fracture stress.

The specimens ZM and C1 showed no cracks. Therefore it was possible to estimate the fracture toughness only for specimens C2 and C3. Specimen C2 (1500°C, 1 h) showed a toughness value of 5·7 MPa $\sqrt{m}$ and specimen C3 one of 7·2 MPa $\sqrt{m}$. It was possible to achieve high green densities (60% by isostatic pressing at 200 MPa) by mixing nano-size ZrO_2 particles (diameter ~17 nm) with micro-scale Al_2O_3 particles (diameter ~600 nm). These specimens sintered to high densities at high temperature without marked grain growth. Furthermore, specimen C (sintered 1 h at 1600°C) attained a high hardness (17·8 GPa) and fracture toughness of 7·2 MPa $\sqrt{m}$ due to the reinforcing effect of ZrO_2 and the high fraction of the tetragonal phase.

References

1. Gleiter, H. & Marquardt, P., Nanokristalline Strukturen—ein Weg zu neuen Materialien? *Z. Metallkunde*, **75** (1984) 263–7.
2. Gleiter, H., Nanocrystalline materials. *Prog. Mat. Sci.*, **33** (1989) 223–315.
3. Tasaki, A., Tomiyama, S. & Iida, S., Magnetic properties of ferromagnetic metal fine particles prepared by evaporation in argon gas. *Japan. J. Appl. Phys.*, **4** (1965) 707–11.
4. Karch, J., Birringer, R. & Gleiter, H., Ceramic ductile at low temperature. *Nature*, **330** (1987) 556–8.
5. Garvie, R. C., Hannink, R. H. & Pascoe, R. T., Ceramic steel? *Nature*, **258** (1975) 703–4.
6. Porter, D. L. & Heuer, A. H., Mechanisms of toughening partially stabilized zirconia (PSZ). *J. Am. Ceram. Soc.*, **60** (1977) 183–4.
7. Gupta, T. K., Lange, F. F. & Bechtold, J. H., Effect of stress-induced phase transformation on the properties of polycrystalline zirconia containing metastable tetragonal phase. *J. Mat. Sci.*, **13** (1978) 1464–70.
8. Lange, F. F., Transformation toughening, Part 1: Size effect associated with the thermodynamics of constrained transformations. *J. Mat. Sci.*, **17** (1982) 225–34.
9. Gupta, T. K., Bechtold, J. H., Kuznicki, R. C., Cadoff, L. H. & Rossing, B. R., Stabilization of tetragonal phase in polycrystalline zirconia. *J. Mat. Sci.*, **12** (1977) 2421–6.
10. Garvie, R. C. & Nicholson, P. C., Phase analysis in zirconia systems. *J. Am. Ceram. Soc.*, **55** (1972) 303–5.
11. Schmidt, H. K., Quantitative analysis of polymorphic mixes of zirconia by X-ray diffraction. *J. Am. Ceram. Soc.*, **70** (1987) 367–76.

12. Granqvist, C. G. & Buhrman, R. A., Ultrafine metal particles. *J. Appl. Phys.*, **47** (1976) 2200–19.
13. Warren, B. E. & Averbach, B. L., The effect of cold-work distortion on X-ray patterns. *J. Appl. Phys.*, **21** (1950) 595–9.
14. Riehemann, W. & Mordike, B. L., Production of powder by irridating surfaces with high power laser beams. In *Laser Treatment of Materials*, ed. B. L. Mordike. DGM-Informationsgesellschaft Verlag, Oberursel, FRG, 1987, pp. 459–66.
15. Fritze, L., Riehemann, W. & Mordike, B. L., Production of ultrafine alumina and zirconia powders by laser induced evaporation. In *International Conference on Powder Metallurgy*, Vol. 3, London, 1990, pp. 23–7.
16. Lee, H.-Y., Riehemann, W. & Mordike, B. L., Grain growth and phase changes during sintering of nanocrystalline zirconia. In *International Conference of Grain Growth in Polycrystalline Materials*, Rome, Centro Sriluppo Materiali Rome, 1991.